Focusing and Scanning Microscopy with Propagating Surface Plasmons

B. Gjonaj,[1,*] J. Aulbach,[1] P. M. Johnson,[1] A. P. Mosk,[2] L. Kuipers,[1] and A. Lagendijk[1]

[1]*FOM-Institute for Atomic and Molecular Physics AMOLF, Science Park 104, 1098 XG Amsterdam, Netherlands*

[2]*Complex Photonic Systems, Faculty of Science and Technology, and MESA+ Institute for Nanotechnology, University of Twente, P.O. Box 217, 7500 AE Enschede, Netherlands*

(Received 18 March 2013; published 26 June 2013)

Here we demonstrate a novel surface plasmon polariton (SPP) microscope which is capable of imaging below the optical diffraction limit. A plasmonic lens, generated through phase-structured illumination, focuses SPPs down to their diffraction limit and scans the focus with steps as small as 10 nm. This plasmonic lens is implemented on a metallic nanostructure consisting of alternating hole array gratings and bare metal arenas. We use subwavelength scattering holes placed within the bare metal arenas to determine the resolution of our microscope. The resolution depends on the size of the scanning SPP focus. This novel technique has the potential for biomedical imaging microscopy, surface biology, and functionalization chemistry.

DOI: 10.1103/PhysRevLett.110.266804 PACS numbers: 73.20.Mf, 68.37.−d, 87.64.M−

In conventional microscopy, features smaller than about half a wavelength cannot be resolved due to the diffraction limit of far-field optics. As the basic constituents of cells and nanotechnological devices are smaller than the wavelength of visible light, a variety of methods [1,2], including scanning near-field nanoprobes [3–5], have been developed for imaging below the diffraction limit. Current far-field methods exploit either the high refractive index of immersion media [6] or the photophysics of molecules [7–10] to obtain high resolution images. Plasmonic structures are envisioned to enable surface-bound imaging with a resolution much below the optical wavelength, and indeed stationary hot spots [11–13] of subwavelength size can be generated from plasmons propagating in such structures. Subwavelength imaging with surface plasmons requires a freely scanned plasmonic focus, which has not been demonstrated up to now.

The novel concept of plasmonic microscopy [14] via the excitation of evanescent waves on metallic nanostructures [15–17] offers not only evanescent out-of-plane resolution (as total internal reflection microscopy [18]) but also a large potential for in-plane superresolution: For a fixed light frequency the wavelength of surface plasmon polaritons (SPPs) is shorter than that of freely propagating photons [19–21]. The main barrier for plasmonic microscopy is the impossibility to use plasmon optics for detection: The readout is always optical. Wide-field plasmonic excitation (unfocused SPPs) yields an image that is limited in resolution by the detection optics.

Enhancing the resolution beyond the limit imposed by the detection optics, or superresolution, is achievable provided that plasmon optics are used to provide tightly confined excitation (e.g., a SPP diffraction limited focus) in a scannable way. Recent theoretical [22–24] and experimental [25,26] developments have shown that plasmonic phase structuring might have the potential for 2D surface microscopy. Nevertheless, due to intrinsic problems of these techniques (the degree of complexity, resolution, field of view, or speed), superresolution plasmonic microscopy has yet to be implemented.

We show here the first plasmonic microscope performing at the SPP diffraction limit by imaging scatterers on top of a metallic film acting as our alternative microscope slide. Specifically, we show that by using phase-structured illumination from a spatial light modulator (SLM) we can create a focus of SPPs below the diffraction limit of the optics and raster scan it to perform microscopy. The combined system of the nanostructure with the phase-structured illumination can be thought of as a deformable plasmonic lens. The size of the SPP focus, which determines the resolution, is the diffraction limit of this plasmonic lens. Because of a shorter plasmonic wavelength and improved numerical aperture, this plasmonic diffraction limit is smaller than the optical diffraction limit. Because of the simplicity of our metallic microscope slide, we can theoretically calculate the required phase profile for focusing. This deterministic approach allows for easy and fast scanning of the focus and, thus, microscopy. Because the method is based only on free-space wave propagation (in 2D) and not on resonant phenomena, our microscope is easy to understand, to implement, and to customize for specific uses.

The requirements for a SPP microscope are to create and position a plasmonic lens and to provide a scanning mechanism for consistent and reproducible imaging of the sample surface. The necessity of the scanning mechanism is understandable when the analogy between a standard 3D lens and the plasmonic 2D lens is made. A 3D lens, which has a focal plane, can achieve 3D imaging only if a scanning mechanism is provided. Similarly, a 2D plasmonic lens with a focal line can achieve 2D imaging only via scanning. Our approach to fulfill the SPP microscope

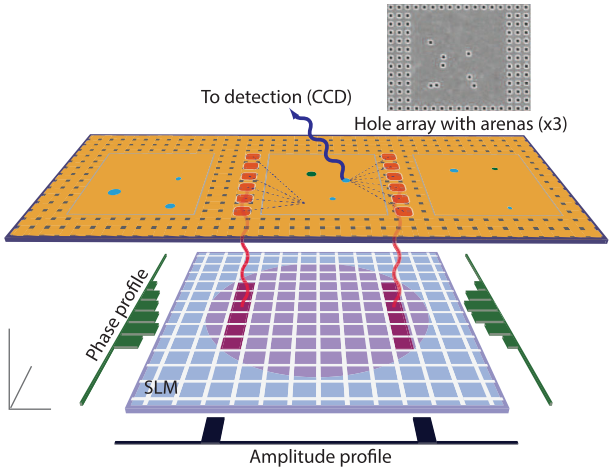

FIG. 1 (color). Working principle of the SPP microscope. The SLM is illuminated with an expanded laser beam (the translucent red circle) and is imaged onto the surface of a nanostructured metallic film. The nanostructure, imaged onto a CCD, is a hole array grating with arenas (grating pitch 450 nm, hole side 177 nm, arena side 5 μm). The arenas consist of bare metal with few scatterers as shown in the inset. Only two pixel lines of the SLM have nonzero amplitude (amplitude profile). These bright pixels, when imaged onto the grating lines adjacent to the arena, locally generate SPPs that propagate into the middle arena. The arena's flatness allows us to predict the phase profile for SPP focusing. Photons are detected only when the SPPs hit a scatterer, thus locating the scatterer. A raster scan (2D) of the focus provides a full SPP resolution image of scatterers.

requirements is (i) to control the amplitude and phase of SPPs locally on the surface of the sample, (ii) to create and raster scan a plasmonic focus in 2D, and (iii) to provide an imaging readout that is fully described by a point-spread function.

To satisfy our first goal we image a SLM onto the surface of the sample, thus mapping each unit cell (pixel) of the SLM to a corresponding area on the sample [26–28]. The image of each pixel (nearly 450 nm in diameter) locally excites surface plasmon waves. These waves propagate along the surface of the sample and are scattered into photons when encountering scattering particles like nanoparticles or fluorescent molecules. Finally, the surface of the sample is imaged onto the sensor of a CCD camera to obtain the spatial distribution of these scatterers.

To achieve SPP focusing at a chosen location we combined our ability to structure the incident illumination (in this case, a He:Ne laser was used) with a specially designed nanostructure. This configuration is schematically depicted in Fig. 1. Two parallel lines of bright pixels (nonzero amplitude) are imaged on a specially designed nanohole array to launch SPP waves. These lines, each comprised of 13 superpixels, are our SPP sources. Each line of sources acts as a phased antenna array that can be modeled to work as a plasmonic lens by using the proper phase of each source.

The area between the source lines, which we will call the arena, is free of the grating: It is bare metal with a few scatterers to test the properties of the microscope. The SPP waves inside the arena can be described by the well known Hankel function (the 2D equivalent of a spherical wave). This knowledge allows us to determine the phases for SPP focusing at any target point inside the arena.

The metallic microscope slide we use is a 5 μm $\times$ 5 μm square arena of homogeneous gold film on glass surrounded by a nanohole array of square holes (hole period of 450 nm and hole sides of 177 nm) in the gold film. In the arena a sparse hole pattern is written as a resolution test and calibration object, as shown in the inset in Fig. 1. Objects in the arena are imaged by using focused SPPs on the gold-air interface. The wavelength of the SPP waves excited by He:Ne light is $\lambda_S = 590$ nm.

To calculate the required phases for focusing at a chosen target point, the distance of all sources from the target must be known. We define a coordination system based on the CCD's pixels and associate pixel coordinates to the sources and the targets. For focusing at the target point $\mathbf{r}_t$, the phase of the nth source determined by the relative distance $r_{t,n}$ is $\tilde{\phi}(\mathbf{r}_n, \mathbf{r}_t) = -2\pi r_{t,n}/\lambda_S$. Finally, to implement the scanning of the focus (required for imaging) we repeat the calculation for a 2D grid of target points.

By raster scanning the SPP focus we image the surface of the sample. A single point of the final image is acquired by focusing the SPP at one target point $\mathbf{r}_t$ having coordinates (x_t, y_t), taking a CCD picture, and reading out only the CCD intensity of the pixel corresponding to those same coordinates. Such a readout is optimal, because it corresponds to a confocal excitation-detection scheme: The microscope's point-spread function (PSF) is the product of the excitation PSF with the detection one. With $h_d(\mathbf{r})$ the detection PSF and $h_e(\mathbf{r} - \mathbf{r}_n)$ the excitation PSF (focused at $\mathbf{r}_t$), the CCD intensity for a delta source is

$$I^t(\mathbf{r}) = [h_e(\mathbf{r} - \mathbf{r}_t)\delta(\mathbf{r})] \otimes h_d(\mathbf{r}) = h_e(-\mathbf{r}_t)h_d(\mathbf{r}). \quad (1)$$

The image of the source that we acquire with our readout while scanning the focus on the grid of target points $\{\mathbf{r}_t\}$ provides the microscope's PSF:

$$\forall t \quad h_m(\mathbf{r}_t) \equiv I^t(\mathbf{r})|_{\mathbf{r}=\mathbf{r}_t} = h_e(-\mathbf{r}_t)h_d(\mathbf{r}_t) \quad (2a)$$

$$\Rightarrow h_m = h_e \cdot h_d, \quad (2b)$$

thus confirming the confocal excitation-detection regime.

The power of two-dimensional imaging using the new scanning plasmon microscope is illustrated in Figs. 2(b)–2(d). For comparison, an image of the same structure obtained with white light illumination is shown in Fig. 2(a). In Fig. 2(b), a portion of the arena is imaged by raster scanning the focus created from a single line of sources above the arena (single lens). In Fig. 2(c), the same portion is imaged with a focus from four lines of SPP sources on all four sides of the arena (2Pi plasmonic lens). At first glance, it is already clear that the plasmonic

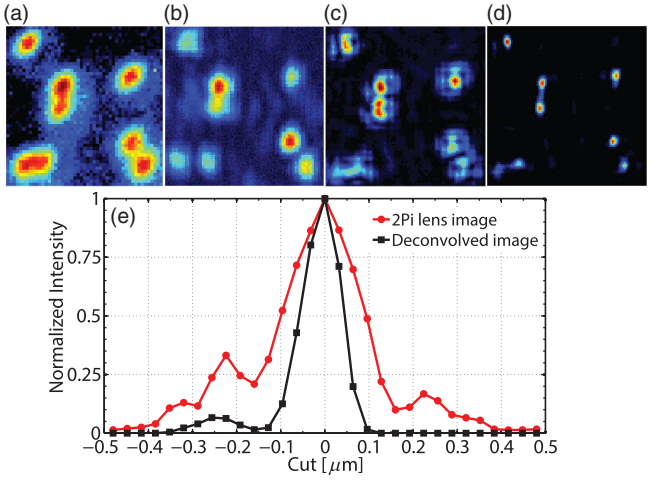

FIG. 2 (color). Imaging the nanostructured arena (3×3 μm fragment). (a) Arena imaged with white light. (b), (c) Imaging the arena via scanning the focus of a (b) single plasmonic lens and (c) 2Pi plasmonic lens. Because of the optimal angular aperture, the 2Pi lens results in sharper focusing and thus imaging resolution. (d) Deconvolution of the 2Pi lens image with a point-spread function assumed as the image of a single nanohole. (e) Linear cuts of an isolated nanohole (top right) before and after deconvolution.

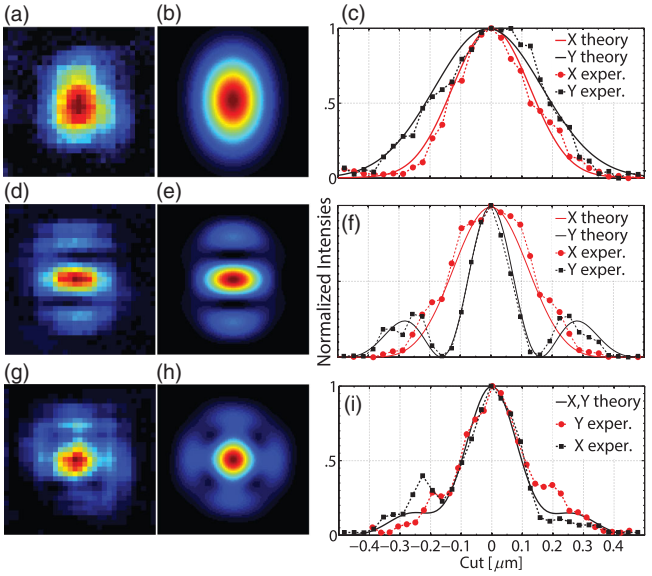

FIG. 3 (color). Evolution of the imaging point-spread function with the lens geometry. Image sizes are 1 μm^2. The first column of images shows the experimental PSFs and the second column the prediction of our theoretical model. The third one compares linear cuts of the two previous columns. (a)–(c) Using a single plasmonic lens above the arena results in an elliptical PSF. (d)–(f) The PSF from a double plasmonic lens (above and below the arena) is still asymmetric but has much sharper features. (g)–(i) The most symmetric PSF is obtained by using the 2Pi plasmonic lens (from two double lenses). For all lenses, the experiments match with the theoretical expectations.

images of the structure are sharper and better resolved than the white light one. The plasmonic images also show that the imaging wave is not deformed by the imaged objects. This is a nontrivial and vital characteristic for proper functioning of the microscope. The 200 nm resolution of Fig. 2(c) is due not only to the SPP wavelength [as for the simple lens of Fig. 2(b)] but also to the optimal plasmonic lens geometry. As shown in Fig. 2(d), an even sharper image is achieved when the 2Pi lens image deconvolved with the PSF (approximated as the image of a single nanohole). This deconvolution image demonstrates that *a posteriori* image processing is feasible. Nevertheless, we define the resolution of our microscope only for unprocessed images using the point-spread function.

The size of the plasmonic focus, which governs the resolution, depends on the SPP wavelength and on the angular aperture of the SPP lens. In our experiment the SPP wavelength is fixed, because it is given by the metal-dielectric interface and the laser frequency. The angular aperture of the SPP lens, however, can be controlled via the illumination geometry (the location of the plasmonic source lines). We have measured and modeled the microscope's PSF for the following geometries: single plasmonic lens from a single source line, double plasmonic lens from two source lines on opposite sides of the arena, and 2Pi plasmonic lens from four source lines surrounding the arena.

The evolution of the microscope's point-spread function with the plasmonic lens geometry, including both the experiment and theoretical results, is shown in Fig. 3. The size of all the images is 1×1 μm^2. In the theoretical model, the PSF is the sum of all source contributions (vectors) from focusing at one target point (the excitation) multiplied with a 2D Gaussian (the detection). The FWHM of the detection point-spread function for the He:Ne wavelength was found to be 430 nm. The acquired image of an isolated nanohole is used as the experimental PSF. In the case of a single plasmonic lens placed above the arena [Figs. 3(a)–3(c)], the PSF is elliptical with FWHMs for the short and long axis of the ellipse given, respectively, by $\lambda_S/2 \approx 300$ nm and the detection resolution of 430 nm (Supplemental Material [29]). For the double plasmonic lens (above and below the arena), the excitation shows plasmonic features along both axis with FWHMs of $\lambda_S/2 \approx 300$ nm and $\lambda_S/4 \approx 150$ nm as shown by Figs. 3(d)–3(f). In Figs. 3(g)–3(i) are shown results for the 2Pi lens geometry. The PSF from the 2Pi lens is almost symmetric with a FWHM of $\lambda_S/3 \approx 200$ nm. For all lens geometries there is excellent qualitative and quantitative agreement between theoretical modeling and experiment.

The theoretical limit to the intensity distribution of the plasmonic excitation is given by the square of the Bessel function J_0 resulting in an excitation FWHM of $\lambda_S/2.8$. Such a theoretical limit corresponds to a complete time reversal mirror [30,31] (Supplemental Material [29]). There is a slight increase to the microscope's PSF above

this theoretical limit of the excitation due to the confocal arrangement. The 2Pi lens roughly matches this resolution. The results suggest that we have reached the limit of the lens geometry. The only parameter left for optimization is the metal-dielectric interface which determines the plasmonic wavelength and losses. Far from the plasmon resonance, for any laser wavelength λ, our model prediction for the resolution of plasmonic microscope (2Pi lens) yields

$$\Delta \equiv \frac{\lambda}{3 \cdot n_S(\lambda)}, \tag{3}$$

with $n_S = \lambda/\lambda_S$ the effective refractive index of the surface plasmons.

The final limitation to the microscope's resolution is due to plasmonic losses which can deteriorate the PSF. Optimal PSFs are achieved for arena sizes smaller than the SPP propagation length, a criteria well satisfied in our experiment. Such criteria can be relaxed if we compensate losses with tunable SLM amplitude. Numerical calculations show that even with arenas several times the propagation length, PSFs with widths equal to those shown in this experiment are achievable providing the sources are tuned to create isotropic illumination of the focus location. The right choice of materials can also optimize the PSF and minimize losses. For example, for the silicon nitrate and silver interface at the laser wavelength of 488 nm, SPPs have a refractive index of $n_s = 2.6$ yielding a resolution of 65 nm and easily manageable losses without shrinking the arena. For more complicated metal-insulator-metal interfaces, even resolutions below 50 nm are predicted.

The resolution is governing the parameter of a microscope, but aberrations, depth of focus, field of view, and acquisition time can be important as well. In principle, for our plasmonic microscope, none of these parameters presents a limitation. The plasmonic lens is created by using phase patterns which are also the basis of an adaptive platform for abberation correction. The depth of focus is, optimally, evanescent. The field of view determines the acquisition time (because of scanning); thus, these two parameters are in conflict with each other. This conflict can be solved by creating in parallel multiple foci in as many arenas. This multiplexing is possible because a megapixel SLM can generate many 2Pi lenses (less than 100 pixels) periodically spaced on a sample with multiple arenas. Thus, the field of view can be extended to multiple arenas without increasing the acquisition time.

In conclusion, we have demonstrated a novel imaging technique based on surface plasmon polaritons that provides resolution beyond optical diffraction without scanning near-field probing, clarifying that SPPs are potentially useful imaging waves for microscopy. The novelty of the method is the use of deformable plasmon optics for 2D imaging, which, in contrast to previous attempts on SPP microscopy with far-field detection, provides resolution dependent on the SPP wavelength. To create the plasmonic lens we use phase-structured illumination from a SLM, deterministic (without feedback) calculation of the phases for focusing, and raster scanning. The geometry of the plasmonic lens is optimized for maximal angular aperture and thus provides the theoretical limit to the resolution.

We thank Hans Zeijlermaker and Dimitry Lamers for sample fabrication. This work is part of the research program of the "Stichting voor Fundamenteel Onderzoek der Materie," which is financially supported by the "Nederlandse Organisatie voor Wetenschappelijk Onderzoek."

*Present address: Department of Electrical Engineering, Technion-Israel Institute of Technology, Haifa 32000, Israel.
b.gjonaj@ee.technion.ac.il

[1] A. Szameit, Y. Shechtman, E. Osherovich, E. Bullkich, P. Sidorenko, H. Dana, S. Steiner, E. B. Kley, S. Gazit, T. Cohen-Hyams, S. Shoham, M. Zibulevsky, I. Yavneh, Y. C. Eldar, O. Cohen, and M. Segev, Nat. Mater. **11**, 455 (2012).
[2] E. T. F. Rogers, J. Lindberg, T. Roy, S. Savo, J. E. Chad, M. R. Dennis, and N. I. Zheludev, Nat. Mater. **11**, 432 (2012).
[3] L. Novotny and B. Hecht, *Principles of Nano-Optics* (Cambridge University Press, Cambridge, England, 2006), p. 558.
[4] M. L. M. Balistreri, H. Gersen, J. P. Korterik, L. Kuipers, and N. F. van Hulst, Science **294**, 1080 (2001).
[5] R. Hillenbrand, T. Taubner, and F. Keilmann, Nature (London) **418**, 159 (2002).
[6] E. G. van Putten, D. Akbulut, J. Bertolotti, W. L. Vos, A. Lagendijk, and A. P. Mosk, Phys. Rev. Lett. **106**, 193905 (2011).
[7] E. Betzig, J. K. Trautman, T. D. Harris, J. S. Weiner, and R. L. Kostelak, Science **251**, 1468 (1991).
[8] S. W. Hell and J. Wichmann, Opt. Lett. **19**, 780 (1994).
[9] E. Betzig, G. H. Patterson, R. Sougrat, O. W. Lindwasser, S. Olenych, J. S. Bonifacino, M. W. Davidson, J. Lippincott-Schwartz, and H. F. Hess, Science **313**, 1642 (2006).
[10] M. J. Rust, M. Bates, and X. Zhuang, Nat. Methods **3**, 793 (2006).
[11] M. Aeschlimann, M. Bauer, D. Bayer, T. Brixner, F. J. G. de Abajo, W. Pfeiffer, M. Rohmer, C. Spindler, and F. Steeb, Nature (London) **446**, 301 (2007).
[12] X. Li and M. I. Stockman, Phys. Rev. B **77**, 195109 (2008).
[13] G. Volpe, S. Cherukulappurath, R. J. Parramon, G. Molina-Terriza, and R. Quidant, Nano Lett. **9**, 3608 (2009).
[14] The use of surface plasmon polaritons for superresolution microscopy as described in this Letter should not be confused with the use of SPPs for detecting small index of refraction changes at low resolution such as described in B. Rothenhäusler and W. Knoll, Nature (London) **332**, 615 (1988).
[15] N. Fang, H. Lee, C. Sun, and X. Zhang, Science **308**, 534 (2005).
[16] F. Wei and Z. Liu, Nano Lett. **10**, 2531 (2010).

[17] D. M. Koller, U. Hohenester, A. Hohenau, H. Ditlbacher, F. Reil, N. Galler, F. R. Aussenegg, A. Leitner, A. Trügler, and J. R. Krenn, Phys. Rev. Lett. **104**, 143901 (2010).
[18] D. Axelrod, J. Cell Biol. **89**, 141 (1981).
[19] E. N. Economou, Phys. Rev. **182**, 539 (1969).
[20] E. Verhagen, J. A. Dionne, L. K. Kuipers, H. A. Atwater, and A. Polman, Nano Lett. **8**, 2925 (2008).
[21] J. A. Dionne, L. A. Sweatlock, H. A. Atwater, and A. Polman, Phys. Rev. B **73**, 035407 (2006).
[22] G. Volpe, G. Molina-Terriza, and R. Quidant, Phys. Rev. Lett. **105**, 216802 (2010).
[23] T. S. Kao, S. D. Jenkins, J. Ruostekoski, and N. I. Zheludev, Phys. Rev. Lett. **106**, 085501 (2011).
[24] G. Bartal, G. Lerosey, and X. Zhang, Phys. Rev. B **79**, 201103 (2009).
[25] P. Zhang, S. Wang, Y. Liu, X. Yin, C. Lu, Z. Chen, and X. Zhang, Opt. Lett. **36**, 3191 (2011).
[26] B. Gjonaj, J. Aulbach, P. M. Johnson, A. P. Mosk, L. Kuipers, and A. Lagendijk, Nat. Photonics **5**, 360 (2011).
[27] B. Gjonaj, J. Aulbach, P. M. Johnson, A. P. Mosk, L. Kuipers, and A. Lagendijk, Nano Lett. **12**, 546 (2012).
[28] E. G. van Putten, I. M. Vellekoop, and A. P. Mosk, Appl. Opt. **47**, 2076 (2008).
[29] See Supplemental Material at http://link.aps.org/supplemental/10.1103/PhysRevLett.110.266804 for more accurate description of the optical configuration, of possible read-outs that will determine the point spread function, as well as some theoretical consideration regarding the interpretation and limits of the method.
[30] J. de Rosny and M. Fink, Phys. Rev. Lett. **89**, 124301 (2002).
[31] R. Carminati, R. Pierrat, J. de Rosny, and M. Fink, Opt. Lett. **32**, 3107 (2007).